Research Article

NMR IN BIOMEDICINE

Received: 26 March 2009, Revised: 21 August 2009, Accepted: 21 August 2009, Published online in Wiley InterScience: 11 November 2009

(www.interscience.wiley.com) DOI:10.1002/nbm.1460

Quantification of brain glycogen concentration and turnover through localized ^{13}C NMR of both the C1 and C6 resonances

Ruud B. van Heeswijk[a], Florence D. Morgenthaler[a], Lijing Xin[a] and Rolf Gruetter[a,b,c]*

We have recently shown that at isotopic steady state ^{13}C NMR can provide a direct measurement of glycogen concentration changes, but that the turnover of glycogen was not accessible with this protocol. The aim of the present study was to design, implement and apply a novel dual-tracer infusion protocol to simultaneously measure glycogen concentration and turnover. After reaching isotopic steady state for glycogen C1 using [1-^{13}C] glucose administration, [1,6-$^{13}C_2$] glucose was infused such that isotopic steady state was maintained at the C1 position, but the C6 position reflected ^{13}C label incorporation. To overcome the large chemical shift displacement error between the C1 and C6 resonances of glycogen, we implemented 2D gradient based localization using the Fourier series window approach, in conjunction with time-domain analysis of the resulting FIDs using jMRUI. The glycogen concentration of 5.1 ± 1.6 mM measured from the C1 position was in excellent agreement with concomitant biochemical determinations. Glycogen turnover measured from the rate of label incorporation into the C6 position of glycogen in the α-chloralose anesthetized rat was 0.7 μmol/g/h. Copyright © 2009 John Wiley & Sons, Ltd.

Keywords: glycogen; turnover; Fourier series window

INTRODUCTION

Glycogen (Glyc) is a macromolecule consisting of linked glycosyl units that serves as a storage molecule for glucose (Glc) in the body. Since it has a much lower concentration in the brain than in tissues such as muscle and the liver, its role as a cerebral energy store has been largely neglected, although over the last decade interest has been renewed for several reasons: not only does it appear to play an active role in brain energy homeostasis (1), it is also involved in such processes as memory formation (2) and neurotransmitter synthesis (3). Additionally, it has been implicated in hypoglycemia unawareness, a dangerous complication often encountered in patients treated with exogenous insulin (4).

Glycogen concentration and its changes are the result of the simultaneous action of synthesis and catabolism (i.e. turnover), which likely regulate the level of brain glycogen in the resting state (1,5). In order to gain insight into the role of glycogen in the abovementioned processes, it is important to determine its concentration and metabolic rates.

Metabolism of glycogen can be assessed by measuring the incorporation of its precursor glucose that has been labeled with an isotope like ^{13}C, ^{3}H or ^{14}C. From the time or rate of label incorporation, turnover times or rates can be determined. Currently, the only method to measure label incorporation into glycogen non-invasively *in vivo* is ^{13}C nuclear magnetic resonance (NMR) (1). Following the infusion of isotopically enriched (IE) [1-$^{13}C_1$] Glc, incorporation of ^{13}C label into Glyc can be measured (6). The IE of the infused glucose is close to 100% to improve the signal-to-noise ratio (SNR) of the NMR measurements of glycogen. However, such measurements of ^{13}C label incorporation may be due to increased Glyc IE or due to a net increase in Glyc concentration.

We have previously shown that the absolute concentration of brain Glyc can be determined from the C1 resonance by 'prelabeling' with [1-^{13}C] Glc, i.e. providing the animal exclusively with food that only contains [1-^{13}C] Glc as a source of carbon prior to the experiment (7) to improve the SNR enough to allow the measurement of the Glyc C1 signal. When the enrichment at C1 reached steady state, the IE of N-acetylaspartate (NAA) was used to determine the IE of Glyc *in vivo*. This approach allowed the measurement of the Glyc concentration while minimally perturbing it (8), but provided no information on turnover.

* *Correspondence to: R. Gruetter, Centre d'Imagerie BioMédicale (CIBM), CH F1 542, Station 6, Ecole Polytechnique Fédérale de Lausanne (EPFL), 1015 Lausanne, Switzerland.*
E-mail: Rolf.Gruetter@epfl.ch

a *R. B. van Heeswijk, F. D. Morgenthaler, L. Xin, R. Gruetter*
Laboratory for Functional and Metabolic Imaging, EPFL, Lausanne, Switzerland

b *R. Gruetter*
Department of Radiology, University of Lausanne, Lausanne, Switzerland

c *R. Gruetter*
Department of Radiology, University of Geneva, Geneva, Switzerland

Contract/grant sponsor: Centre d'Imagerie BioMédicale (CIBM) of the UNIL, UNIGE, HUG, CHUV, EPFL.
Contract/grant sponsor: Leenaards and Jeantet Foundations.
Contract/grant sponsor: NIH; contract/grant number: R01NS42005.
Contract/grant sponsor: SNSF; contract/grant number: 3100A0-122498.

Abbreviations used: *CSD, chemical shift displacement; CSI, chemical shift imaging; FOV, field of view; FSW, Fourier series window; Glc, glucose; Glyc, Glycogen; IE, isotopically enriched; NAA, N-acetylaspartate; NMR, nuclear magnetic resonance; SNR, signal-to-noise ratio; VOI, voxel of interest.*

NMR IN BIOMEDICINE

However, if after this prelabeling [1,6-$^{13}C_2$] Glc is infused at the IE of the Glyc C1 resonance, the C1 resonance will remain in isotopic steady state and will act as a pure concentration change monitor, while the C6 resonance signal will increase mostly due to label incorporation, and can in principle be monitored to determine the turnover time. The aim of the present study was therefore to establish the simultaneous measurement of the glycogen C1 and C6 resonances, such that the C1 resonance can be used to determine concentration and the C6 resonance can be used to determine the turnover time.

One of the challenges of measuring the Glyc C1 and C6 resonances simultaneously is that they are separated by ~4 kHz at 9.4 T due to their chemical shifts of 100.5 and 61.4 ppm respectively. Such a large frequency difference represents a formidable challenge for 3D spatial localization using gradient-based methods, to date the only method capable of measuring NMR of Glyc in the brain. To overcome chemical shift displacement (CSD), one of the goals of the present study was therefore to implement a new gradient-based localization sequence that aimed to minimize CSD: the two-dimensional Fourier series window (FSW, (9)).

Fourier series window (FSW) based pulse sequences have been used mostly for ^{31}P NMR in muscle and liver (10–12). The FSW is an alternative to traditional Fourier transform chemical shift imaging (CSI). A predetermined voxel shape is chosen for which a single window *W* (the voxel) of resolution N is generated by summation of $2N+1$ phase-encoded FIDs that are multiplied by a series of matching Fourier coefficients β_n (see Appendix for a recapitulation of FSW theory).

The FSW localization approach can be tailored to achieve arbitrary voxel shapes, has low cross-voxel contamination and a complete lack of CSD (13). The number of repetitions per phase encoded FID should correspond to the Fourier coefficient's relative weight; a phase encode with a low Fourier coefficient will need only a few averages, while a high coefficient should imply many averages for efficient performance. The FSW approach is thus ideally suited for applications that require many averages as is the case for ^{13}C NMR of glycogen.

Therefore the aim of the present study was two-fold: first to implement a localization scheme based on the 2D Fourier series window to minimize CSD, and second to establish a dual-isotope protocol using [1,6-$^{13}C_2$] glucose and to determine the Glyc turnover time while monitoring its concentration under light anesthesia.

METHODS

NMR instrumentation

All experiments were performed using an actively shielded 9.4 T 31 cm horizontal-bore Varian spectrometer with high-performance gradients (400 mT/m in 130 μs). A custom-built 3-loop 10 mm diameter surface coil was used for ^{13}C excitation and detection, while quadrature 14 mm ^{1}H coils were used for positioning, shimming and decoupling (14). Shimming was performed with FASTMAP (15).

FSW pulse sequence

The total delay for the gradients to play out between the excitation pulse and the start of the acquisition was 270 μs (Fig. 1), which should result in less than 3% signal loss due to the estimated glycogen T_2 of 10 ms (16). Slice selection in the third dimension was achieved using one-dimensional ISIS (17), using a 6 ms hyperbolic secant pulse to select a slice of 1 cm thickness. The ISIS localization is prone to signal reduction because of the short relaxation times of glycogen; the Glyc signal reduction due to ISIS was experimentally determined to be less than ~10% in 1D localized volumes encompassing the entire sensitive volume of the ^{13}C RF coil. The gradient strength was set to 125 mT/m, which for the ^{13}C gyromagnetic ratio of 10.7 MHz/T is equivalent to 13.4 kHz/cm. The chemical shift difference of 3.9 kHz between the Glyc C1 and C6 resonances will therefore result in a chemical shift displacement of 3.9/13.4 = 0.3 cm. A minimum of two averages was thus required per gradient setting. We propose the acronym FOSSIL (Fourier Series-based Spectroscopic Imaging Localization) for this 2D Fourier.

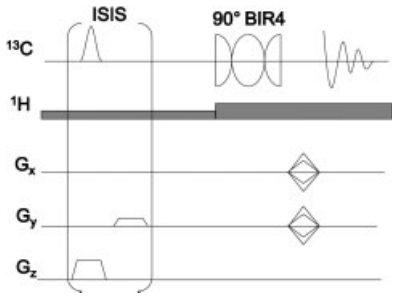

Figure 1. Diagram of the FOSSIL pulse sequence. The 90° BIR-4 pulse is preceded by a 1D ISIS module for slice selection. The time between the BIR-4 and the acquisition was 270 μs, while the repetition time was 10 s for the phantom and 1 s for the rat.

WALTZ-16 broadband NOE and decoupling were applied at the ^{1}H water frequency (18). A 3 ms 90° BIR-4 pulse (19) was used for excitation, with a nominal bandwidth of 5 kHz at 2.5 kHz γB_{1max}, sufficient to cover the 3.9 kHz frequency difference between the Glyc C1 and C6 resonances (Fig. 2). The 3 ms BIR-4 pulse was assessed to result in less than ~4% Glyc signal reduction in unlocalized spectra. The phase of the BIR-4 pulse increasingly varies nearer to the edge of its nominal bandwidth.

The Fourier coefficients were calculated (see Appendix) for a square two-dimensional Fourier series window in two dimensions with a field of view (FOV) of 22×22 mm^2. For a window resolution of 1/5 FOV (4.4×4.4 mm^2) and $n = 5$ coefficients this resulted in $(2N+1)^2 = 121$ phase encodes, while for 1/8 FOV (2.75×2.75 mm^2) and $n = 8$ coefficients it resulted in 289 phase encodes. Each of these phase encodes had its number of acquisitions adapted to its 2D Fourier coefficient β_n (Eq. A.5 in the Appendix).

Validation of FSW localization in phantom experiments

To verify the localization accuracy of the FSW sequence, we used a seven-compartment phantom, consisting of a water-filled Perspex half-cylinder in which 6 tubes with different solutions were mounted. The tubes contained saturated solutions of either bicarbonate (of which the carboxyl carbon resonates at 168.9 ppm), formate (174.0 ppm), carbonate (161.1 ppm) or acetate (182.2 ppm).

The repetition time was set to 10 s as a compromise between the long T_1 relaxation time of the carboxyl groups (6–30 s) and limited acquisition time. The average number of acquisitions per gradient setting was 12, adjusted according to the relative coefficient weight (see Appendix).

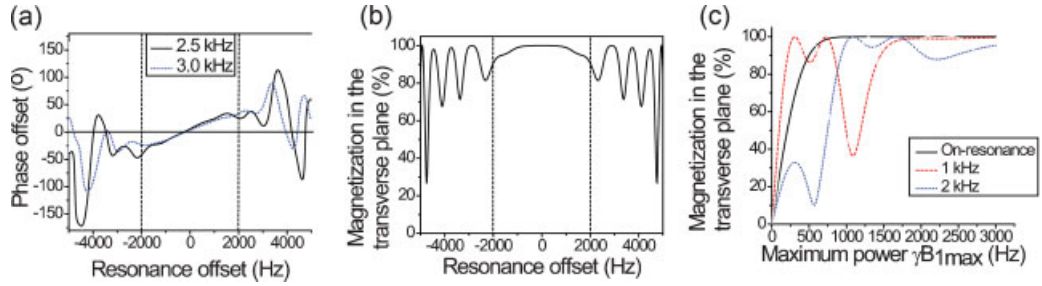

Figure 2. Simulated characteristics of a 3 ms 90° BIR-4 adiabatic pulse: a) resonance offset vs phase offset at different values of γB_{1max}, with horizontal markers at 4 kHz bandwidth. Not far outside the bandwidth, the relation becomes incoherent; b) resonance offset vs magnetization in the transverse plane at 2.5 kHz; outside a bandwidth of roughly 4.5 kHz the flip angle becomes incoherent; c) pulse power vs magnetization in the transverse plane. 2 kHz γB_{1max} appears to be sufficient power for all offsets.

In vivo measurements

To determine the brain Glyc turnover rates and concentrations, six Sprague-Dawley rats (~225 g, Charles River Laboratories, France) were fasted overnight (Fig. 3). The next morning, 24 h before the start of the NMR experiments, they were fed 100% enriched, 10% w/v [1-$^{13}C_1$] Glc in tap water ad libitum to achieve isotopic steady state for the Glyc C1 resonance (without disturbing the Glyc concentration itself and in the case of near-complete turnover) as described previously (7,8).

On the day of the NMR measurement, the animal was anesthetized with 2% isoflurane. Both femoral veins and a femoral artery were catheterized for infusion of glucose and α-chloralose, and blood-gas analysis respectively. After surgery, anesthesia was switched to α-chloralose (an initial bolus of 80 mg/kg followed by continuous infusion of 50 mg/kg/h with 5 mg/ml α-chloralose in saline) under assisted breathing, considered relatively light anesthesia (20). The animal was then placed in the NMR scanner where its temperature was kept at 37.5 ± 0.5°C with circulating warm water. While the animal was in the scanner, blood samples were taken for blood-gas and glycemia analysis every 30 min to monitor physiology.

Glycogen NMR studies

Two sets of 'baseline' datasets with the FSW-based sequence were acquired to determine the glycogen and glucose levels at steady state. With a repetition time of 1 s (taking the Glyc T_1 of ~300 ms at 9.4 T into account (16)), averaging of the phase encodes at 5 coefficients per dimension for a 1/5 FOV window (see Appendix) was calculated such that the total acquisition time was 59 min (see Appendix). The ^{13}C carrier frequency was placed in the center of the Glyc C1 and C6 resonances, while broadband decoupling was applied at the Glc ^1H frequency.

After these baseline acquisitions, a bolus of 0.6 mg/kg [1,6-$^{13}C_2$] Glc whose IE matched that of Glyc C1 was given over 5 min, and a variable-rate infusion of [1,6-$^{13}C_2$] Glc was used afterwards to maintain blood Glc level at 10 mM. Seven more 5×5 FSW datasets were then acquired with a temporal resolution of 1 h.

Figure 3. Overview of the experimental protocol and its timing. After fasting, the animal is prelabeled with C13 Glc, prepared for the study and inserted in the scanner, where its IE is determined. The main study itself then starts and lasts until sacrifice. After the study a phantom is inserted for absolute quantification purposes.

After the study, the animal was sacrificed using 2 s of focused 4 kW microwave radiation (Gerling Applied Engineering, Modesto, CA). The brain was taken out and stored at −80°C for later biochemical determination of Glyc content and high resolution NMR determination of Glyc IE.

A phantom containing 500 mM Glyc (Sigma-Aldrich, St. Louis, MO) and 5 mM [1-^{13}C] Glc was then placed under the coil at T = 37°C, and another set of 5×5 FSW was acquired for absolute quantification purposes as described previously (7).

Isotopic enrichment

The IE of the steady state Glyc C1 position was determined *in vivo* to match the IE of infused Glc to this IE and thus to keep the Glyc C1 IE constant. Since the steady state IE of glycogen using this protocol was empirically established to be 2.2 times that of N-acetylaspartate (NAA) (7), the NAA IE was determined by comparing the ^{13}C-coupled ^1H NAA doublet signals to that of the ^{12}C-coupled ^1H NAA singlet in a modified ACED-STEAM (21) sequence as described previously (7).

Brain extract measurements

The extracted brains were homogenized and prepared for Glc concentration measurement as well as verification of the IE as previously described (8). Briefly, after powderizing the brain by mortar and pestle, 200 µl of 0.03 M sodium acetate was added, which was then homogenized with an ultrasonic processor. The sample was divided into two aliquots, one of which was incubated at 37°C with α-1,4- α-1,6-glucosidase, which completely degrades the glycogen molecule to glucose (22), while the other was incubated with a saline solution. From the glucose content measured in a glucose analyzer (GM7 Micro-stat, Analox Instruments, London, UK), one aliquot effectively gave the summed glucose and glycogen concentration, while the other gave the free tissue glucose concentration. After filtering, lyophilizing and resuspension in D_2O, high-resolution ^1H NMR spectra of these samples were obtained at 600 MHz. The ratio of the ^{13}C bound doublet and ^{12}C-bound singlet were used to calculate the IE of free glucose in one aliquot, and the concentration-weighted average IE of Glc and Glyc in the other. The free glucose IE was then used to calculate the Glyc IE from the concentration-weighted average IE of Glc and Glyc using Eq. 3 from Ref. (7).

Spectral processing

The calculation of the localized FIDs from the coefficient weighted individual FSW FIDs was done in MATLAB (The Mathworks Inc., Natick, MA, USA) using Eq. A.3 in the Appendix. The datasets were reconstructed into a grid of 16×16 to allow the selection of an optimally positioned voxel for every study. The resulting FIDs were subsequently DC corrected and multiplied with a 15 Hz exponential decay.

The localized FIDs were processed in the time-domain using the jMRUI software package (23,24). A frequency filter was applied to select the chemical shift range from 47–110 ppm. A total of 10 signal components were fitted using AMARES (Advanced Method for Accurate, Robust, and Efficient Spectral fitting) (25): Glyc C1, Glc C1β, Glc C1α, glycerol C1, Glc C6, Glyc C6, a peak each for glutamine C2, glutamate C2 and aspartate C2, plus a term accounting for any residual DC offset. The linewidths of glucose (C1α, C1β and C6) were constrained to be equal, and the linewidths of Glyc C1 and C6 were constrained to be equal. These constraints on Glyc C6 and Glc C6 allowed separate quantification of the overlapping C6 resonances of Glc and Glyc. Since the phase of each individual resonance was stable throughout the experiment, the phase was estimated for each animal from the summed time series; the phase however varied along the spectrum due to the phase profile of the BIR-4 excitation pulse (Fig. 2a). To minimize the influence of the broad baseline components, the first 10 data points of the signals were weighted with a quarter-sine wave (25).

Quantitation and turnover calculation

Absolute concentrations of Glc C1, Glyc C1 and Glyc C6 were calculated from the *in vivo* and phantom signals *S*, the signals of the formic acid reference phantom in both situations (to correct for RF loading) and a correction factor α for differences in NOE and partial T_1 relaxation as in previous studies ((26) and references therein). This results in:

$$[Gl]_{iv} = \frac{S_{Gl,iv}}{S_{Gl,ph}} \frac{S_{FA,iv}}{S_{FA,ph}} \alpha \frac{1.1\%}{IE_{Gl,iv}} [Gl]_{ph}. \quad (1)$$

Here the *Gl* and *FA* are glucose/glycogen and formic acid, while iv and ph are *in vivo* and phantom.

A basic model consisting of Glyc, Glc and their intermediary glucose-6-phosphate (G6P) was used to model the Glyc C6 labeling time course. It was assumed that labeled Glc increased stepwise at $t = 0$, that there was no Glyc label at $t = 0$ (1.1% natural abundance neglected) and that the Glyc concentration does not change over time. The corresponding set of differential equations was then solved for the C6-labeled Glyc concentration over time C(t) as described in Ref. (27), which resulted in:

$$C(t) = [Glyc]_{C6} * (1 - \exp[-t/\tau]), \quad (2)$$

where $[Glyc]_{C6}$ is the steady state Glyc C6 concentration and τ is the Glyc turnover time. This equation was then used to fit the Glyc C6 time course.

The Glc C1 and Glyc C1 time courses were fitted to a linear curve. If the slope of the curve was more than an order of magnitude lower than its fitting error, the time course was fitted with a constant instead. All time courses were fitted with OriginPro (OriginLab Corporation, Northampton, MA, USA).

RESULTS

The localization ability of the 2D FSW sequence was tested on a phantom containing bicarbonate, formate, carbonate and acetate (Fig. 4). Despite the range of 20 ppm in chemical shift, the FSW signals of a formate, carbonate and acetate compartment overlap with their ^{1}H image equivalents, as evidenced from the FSW color maps of the resonances projected on top of a ^{1}H gradient echo image (Fig. 4b). Note that the compartments that were more than ~10 mm away from the surface coil plane were outside the sensitive volume of the small ^{13}C coil and thus not detected.

Localization of the 2D FSW sequence was further tested *in vivo*. Since it is well established that ^{13}C resonances from lipids originate outside the brain, good localization should eliminate lipid-specific resonances. When placing the voxel of interest (VOI) into superficial regions encompassing fat and muscle, clear resonances ascribed to extra-cerebral fat (glycerol C1,3 at 62.5 ppm) were detected (Fig. 5b). Moving the VOI into the brain minimized the glycerol resonance (Fig. 5c).

The bandwidth of the BIR-4 pulse was ~5 kHz, sufficient to simultaneously excite the Glyc C1 and C6 resonance with less than 10% signal loss (compensated for in the absolute

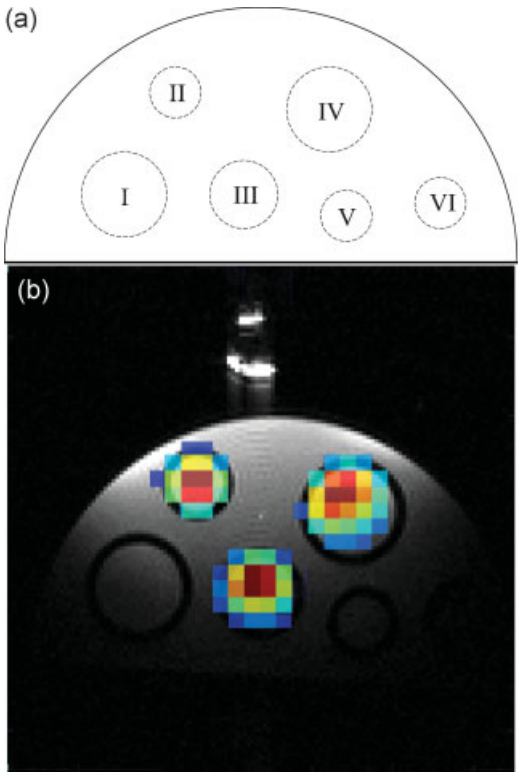

Figure 4. The localization capacity of the FSW sequence: a) schematic drawing of the 30 mm wide and 52 mm long half-cylindrical localization phantom. The compartment diameters and solutions are: I. 6 mm filled with bicarbonate, II. 4 mm filled with formate, III. 5 mm filled with carbonate IV. 6 mm filled with acetate V. 4 mm filled with bicarbonate and VI. 4 mm filled with formate. The detection coil was placed on top of the phantom; b) Thresholded ^{13}C FSW color maps of the different resonances have been projected on top of a ^{1}H gradient echo image. From left to right the color maps are formate, carbonate and acetate, all scaled to fit the same color range. The locations of the individual compartments can be seen in the gradient echo image, as can parts of the formic acid-filled bubble at the center of the coil.

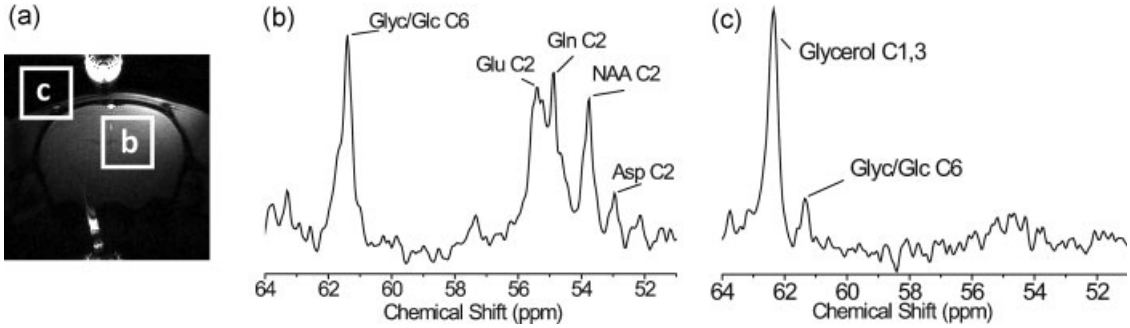

Figure 5. Demonstration of the FSW sequence localization capability: a) ^{1}H gradient echo image with the same FOV size as the FSW sequence (22×22 mm^2) and the positions of two windows indicated with white rectangles; b) example of a localized spectrum in the brain. Note the presence of cerebral metabolites and the large Glc/Glyc peak; c) localized spectrum outside the brain; in this case in the skin. Notice that the relative contribution of the glycerol is much bigger than that of Glyc and Glc C6, which still has a small presence due to the partial location of the voxel in the brain.

quantification procedure), according to simulations (Fig. 2) and verified in phantom studies. Since the RF coil's RF loading varied per subject, the effective power for the 90° BIR-4 RF pulse was varied slightly each time, causing the zero and first order phase of the spectra to vary slightly from study to study, as expected from the pulse profile (Fig. 2b). Therefore, while the magnitude of the excited signal for the resonances of interest was comparable across all studies, the phase over the entire spectrum varied up to 70°. In particular, the phase of the Glyc C1 and Glyc/Glc C6 resonances, while stable per subject, showed large variations across subjects. Nonetheless, the SNR of the localized spectra was in all cases high enough to allow robust fitting using the time-domain AMARES fitting routine, including the aforementioned phase variations, resulting in negligible residuals over the spectral regime of interest (Fig. 6).

The time courses of the Glyc and Glc C1 signal were within experimental error constant, consistent with the isotopic steady-state achieved using this protocol (Fig. 7). For the quantitation, both C1 resonances were corrected for the IE (measured from NAA as in our previous study), which was established at $IE_{Glyc,inv} = 42 \pm 6\%$. The *in vivo* IE determination was within a few percent comparable to that in brain extracts (as previously, (7)): a linear fit through the origin resulted in $IE_{Glyc,invivo} = 1.03 \cdot IE_{Glyc,highres}$ ($R^2 = 0.98$, $p = 0.16$).

From the thus determined IE of Glyc and the [1-^{13}C] Glyc concentration measured by *in vivo* NMR, the total concentration of glycogen and glucose was calculated using Eq. 1, resulting in total Glc and Glyc concentrations of $[Glc]_{t,C1} = 4.3 \pm 1.0$ and $[Glyc]_{t,C1} = 5.1 \pm 1.6$ mM respectively. Here the subscript t stands for total, while C1 indicates that the concentration was based on the integral of the C1 resonance. The determined glycogen concentrations were, within experimental error, identical to that determined by concomitant biochemical assays, which yielded $[Glyc]_{t,assay} = 5.3 \pm 1.6$ mM.

The Glc C6 signal increased in a step-like manner to reach steady state levels within 30 min after the start of the [1,6-$^{13}C_2$] Glc infusion at $t = 0$, whereas the Glyc C6 signal slowly increased over time. Given that the stability of Glyc C1 indicated minimal concentration changes, this gradual increase in the Glyc C6 signal therefore mainly represents changes in the IE of Glyc C6, and thus can be used to estimate glycogen turnover time.

An exponential fit of the Glyc C6 signal with Eq. 2 resulted in a turnover time of 8 ± 4 h ($R^2 = 0.97$) and a steady state Glyc C6 concentration of $[Glyc]_{C6} = 3 \pm 1$ mM. Dividing the steady state concentration of the Glyc C6 time course by its IE (assuming the same C6 IE at steady state as the C1 resonance) resulted in a total glycogen concentration $[Glyc]_{t,C6} = 7 \pm 3$ mM. By dividing the average $[Glyc]_t$ by τ we calculated a Glyc turnover rate of 0.7 ± 0.6 μmol/g/h. Constraining $[Glyc]_{C6}$ to the Glyc C1 concentration ($[Glyc]_{t,C1}$*IE = 5.3*0.41 = 2.2 mM) and fitting the same function resulted in $\tau = 5.2 \pm 0.4$ h.

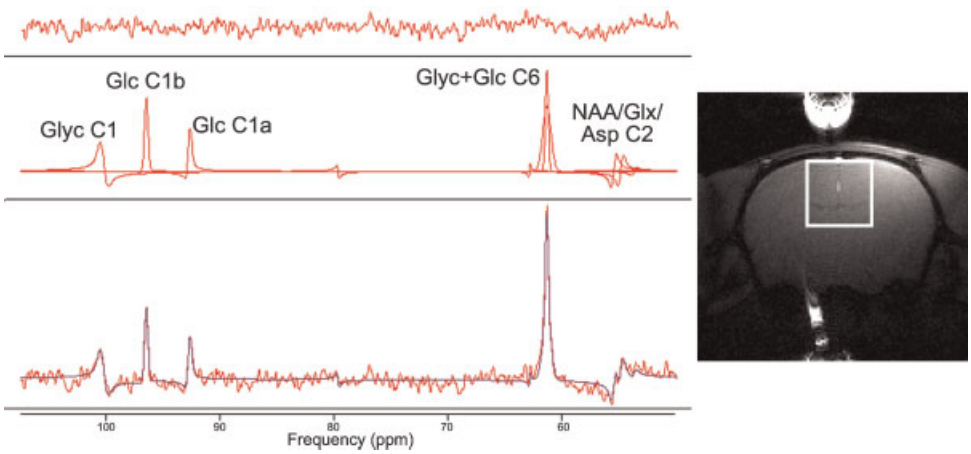

Figure 6. jMRUI fitting of a FSW brain spectrum after 6 h of infusion. Bottom: spectrum and fit. Middle: individual peaks with their names. Top: fit residual. Image: location of the window within the brain, with a formic acid phantom visible at the center of the detection coil.

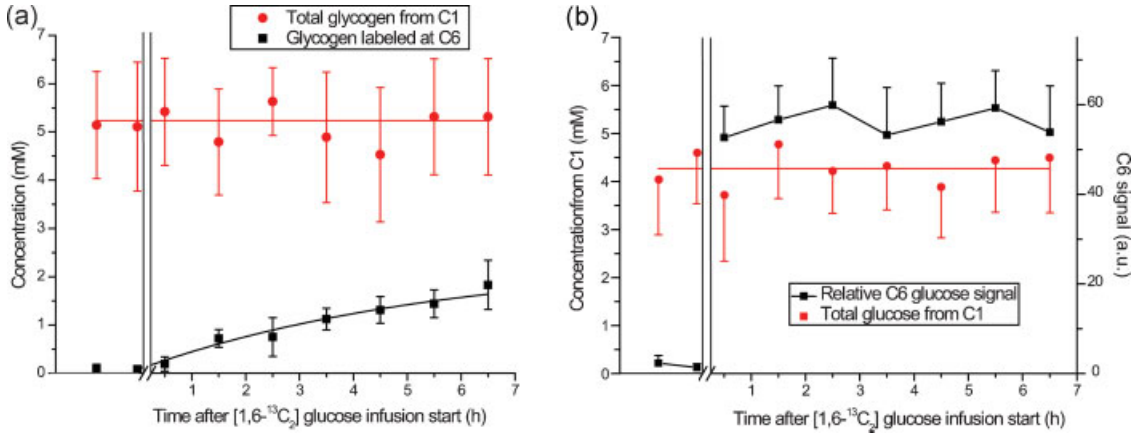

Figure 7. Time courses of the Glyc and Glc resonances; a) the total Glyc concentration as calculated from the C1 resonance (circles) with its linear fit, as well as the increasing concentration of Glyc that is labeled at the C6 resonance (squares); b) The total Glc concentration as calculated from the C1 resonance (circles; scale on the left side) as well as the Glc C6 resonance signal strength (scale on the right side). Note that the Glc C6 is not quantified and thus has an arbitrary scale. All errors bars are SD over the different animals.

DISCUSSION

In this study we implemented and used the FSW approach for the first time for 2D localization of ^{13}C signals, which, combined with a novel dual isotope infusion protocol, allowed the simultaneous determination of Glyc concentration and turnover.

While the dephasing that the phase encoding generates implies that the 2D FSW pulse sequence is theoretically not as efficient as single-voxel localized spectroscopy, the sequence does have the same efficiency equivalent to conventional spectroscopic imaging, provided that the amount of acquisitions per gradient setting are weighted by their Fourier coefficient. Therefore, the SNR per time unit observed in the present study was ~70% that of single-voxel ^{13}C spectroscopy studies (7,18). The sequence appears to be a suitable alternative for regular spectroscopic imaging or localized spectroscopy if large chemical shift ranges are to be localized, provided sufficient averaging is performed.

Time-domain fitting of the spectra was robust: the phase variations across the chemical shift of the FSW spectra were expected from the simulations of the BIR-4 pulse and were easily accounted for by the AMARES routine. The step-like increase of Glc C6 at the start of the infusion together with the slow increase of Glyc C6 over time indicated that their resonances were robustly deconvolved based on their substantially different linewidths, despite Glyc and Glc C6 having considerable spectral overlap.

The 2D FSW pulse sequence was combined with the IE determination and external reference quantification to obtain absolute quantifications of Glyc. IE determination was in excellent agreement with previous results (7,26), and the *in vitro* biochemistry and high resolution ^{1}H NMR confirmed the validity of the *in vivo* method.

The absolute quantification of the C1 resonance resulted in total Glc and Glyc concentration time that were constant over time, indicating stable Glyc and Glc concentrations, the former validated by biochemical *in vitro* analysis and in agreement with previously reported levels under similar hyperglycemic and anesthetic conditions (8). Due to the slightly hyperglycemic level at which the blood glucose was maintained, a slight increase in the Glyc concentration over time could also have been expected. This was, however, not observed, which may be due to SNR being too low to detect such a small increase: a linear Glyc C1 time course fit in which the slope was left free resulted in a slope of $-8 \times 10^{-4} \pm 0.25$ mM/h, showing that a glycogen concentration increase of at least 0.5 mM/h was necessary to be statistically significant.

CONCLUSIONS

We conclude that a) Glyc C1 and C6 can be simultaneously measured *in vivo* using the FSW based pulse sequence, and that b) the dual isotope infusion protocol proposed can be used to simultaneously determine both the Glyc concentration and turnover *in vivo*.

Acknowledgements

The authors would like to thank Dr Paul Vasos for his help with the high resolution spectrometer, and Ms. Hanne Frenkel and Dr Agathe Python for their veterinary assistance. Supported by Centre d'Imagerie BioMédicale (CIBM) of the UNIL, UNIGE, HUG, CHUV, EPFL and the Leenaards and Jeantet Foundations; NIH grant R01NS42005 and SNSF grant 3100A0-122498.

APPENDIX: FSW THEORY AND CALCULATIONS

The FSW approach has in NMR mostly been used for ^{31}P spectroscopic imaging. A more in-depth treatment of the theoretical background can be found in Refs (9,11,13,28). For convenience, a short overview of this theory is given in this appendix.

In a one-dimensional FSW pulse sequence a predetermined window shape W (the voxel) is chosen with a resolution N and window width FOV/N. A phase encoding gradient is applied to the transverse magnetization such that distance becomes equivalent to the phase φ. The window itself can then be described as a set of $2N + 1$ Fourier coefficients β_n such that in the

one-dimensional case it looks like (9):

$$W(\varphi) = \sum_{-N}^{N} \beta_n e^{in\varphi}. \quad \text{(A.1)}$$

To determine the coefficients β_n, one can reverse Eq. A.1 and integrate from $-\pi$ to π:

$$\beta_n = \frac{1}{2\pi} \int d\varphi W(\varphi) e^{-in\varphi}. \quad \text{(A.2)}$$

To avoid repeating the window inside the FOV, the first coefficient β_1 is set to have an accompanying phase encoding step which has a phase spread of 180° over the FOV. When applied to the spatially encoded MR signal $\rho(\vec{r}, t)$, the window is convolved with a series of phase-encoded FIDs *S(n,t)*:

$$\int d\vec{r} \rho(\vec{r}, t) W(\varphi) = \sum_{-N}^{N} \beta_n S(n, t). \quad \text{(A.3)}$$

The window can be arbitrarily shifted a distance ψ by multiplying the window with $e^{-in\psi}$ (i.e. Fourier shifting). The windowed spatially encoded time-domain signal is now:

$$\begin{aligned} \int d\vec{r} \rho(\vec{r}, t) W(\varphi + \psi) &= \int d\vec{r} \rho(\vec{r}, t) \left[\sum_{-N}^{N} \beta_n e^{in(\psi+\varphi)} \right] \\ &= \sum_{-N}^{N} \beta_n S(n, t) e^{in(\psi)}. \end{aligned} \quad \text{(A.4)}$$

With these equations the parameters for the window of choice can be calculated. In these studies, a square window shape was chosen, so Eq. A.2 was solved for the square shape with width *w*, resulting in 1D coefficients β_n:

$$\beta_n = \frac{\sin(nw/2)}{n\pi}. \quad \mathrm{n} = -\mathrm{N}, -\mathrm{N}+1, \ldots, 0, \ldots \mathrm{N}-1, \mathrm{N} \quad \text{(A.5)}$$

The $2\mathrm{N}+1$ coefficients for the phase encoding combinations can now be calculated. N is usually chosen such that the resolution is FOV/N. The resulting voxel is only approximately rectangular due to truncation by the finite number of coefficients. However, terminating the coefficient function of Eq. A.4 at the first zero crossing (i.e. where $n = \pm 2\pi/w$) substantially reduces any truncation effects (28). The shape of the window results in a slightly larger area than its nominal width, yet 99% of the window intensity drops off at 1.4 times the window width. The 2D FSW separately applies the above equations to the second dimension coefficients β_m as well, resulting in $(2\mathrm{N}+1)^2$ doubly weighted phase encodes.

REFERENCES

1. Gruetter R. Glycogen: the forgotten cerebral energy store. J. Neurosci. Res. 2003; 74(2): 179–183.
2. Gibbs ME, Anderson DG, Hertz L. Inhibition of glycogenolysis in astrocytes interrupts memory consolidation in young chickens. Glia. 2006; 54(3): 214–222.
3. Brown AM, Sickmann HM, Fosgerau K, Lund TM, Schousboe A, Waagepetersen HS, Ransom BR. Astrocyte glycogen metabolism is required for neural activity during aglycemia or intense stimulation in mouse white matter. J. Neurosci. Res. 2005; 79(1–2): 74–80.
4. Cryer PE. Mechanisms of hypoglycemia-associated autonomic failure and its component syndromes in diabetes. Diabetes. 2005; 54(12): 3592–3601.
5. Brown AM, Tekkok SB, Ransom BR. Glycogen regulation and functional role in mouse white matter. J. Physiol. 2003; 549(Pt 2): 501–512.
6. Choi IY, Gruetter R. In vivo 13C NMR assessment of brain glycogen concentration and turnover in the awake rat. Neurochem. Int. 2003; 43(4–5): 317–322.
7. Morgenthaler FD, van Heeswijk RB, Xin L, Laus S, Frenkel H, Lei H, Gruetter R. Non-invasive quantification of brain glycogen absolute concentration. J. Neurochem. 2008; 107(5): 1414–1423.
8. Morgenthaler FD, Koski DM, Kraftsik R, Henry PG, Gruetter R. Biochemical quantification of total brain glycogen concentration in rats under different glycemic states. Neurochem. Int. 2006; 48(6–7): 616–622.
9. Garwood M, Schleich T, Ross BD, Matson GB, Winters WD. A modified rotating frame experiment based on a Fourier-Series Window Function—application to invivo spatially localized NMR-spectroscopy. J. Magn. Reson. 1985; 65(2): 239–251.
10. Garwood M, Schleich T. Improved fourier series windows for localization in in vivo NMR spectroscopy. J. Magn. Reson. 1985; 65: 510–515.
11. Hendrich K, Merkle H, Weisdorf S, Vine W, Garwood M, Ugurbil K. Phase-modulated rotating-frame spectroscopic localization using an adiabatic plane-rotation pulse and a single surface coil. J. Magn. Reson. 1991; 92(2): 258–275.
12. Garwood M, Ugurbil K, Schleich T, Sublett E, From A. In vivo spatially localized surface-coil NMR spectroscopy utilizing a fourier series window function and two surface coils. J. Magn. Reson. 1986; 69: 576–581.
13. Hendrich K, Hu XP, Menon RS, Merkle H, Camarata P, Heros R, Ugurbil K. Spectroscopic imaging of circular voxels with a 2-dimensional Fourier-Series Window technique. J. Magn. Reson. Ser. B. 1994; 105(3): 225–232.
14. Adriany G, Gruetter R. A half-volume coil for efficient proton decoupling in humans at 4 tesla. J. Magn. Reson. 1997; 125(1): 178–184.
15. Gruetter R. Automatic, localized in vivo adjustment of all first- and second-order shim coils. Magn. Reson. Med. 1993; 29(6): 804–811.
16. Overloop K, Vanstapel F, Van Hecke P. 13C-NMR relaxation in glycogen. Magn. Reson. Med. 1996; 36(1): 45–51.
17. Ordidge RJ, Connelly A, Lohman JAB. Image-Selected Invivo Spectroscopy (ISIS)—a new technique for spatially selective NMR-spectroscopy. J. Magn. Reson. 1986; 66(2): 283–294.
18. Choi IY, Tkac I, Gruetter R. Single-shot, three-dimensional 'non-echo' localization method for in vivo NMR spectroscopy. Magn. Reson. Med. 2000; 44(3): 387–394.
19. Garwood M, Yong K. Symmetrical pulses to induce arbitrary flip angles with compensation for Rf inhomogeneity and resonance offsets. J. Magn. Reson. 1991; 94(3): 511–525.
20. Choi IY, Lei H, Gruetter R. Effect of deep pentobarbital anesthesia on neurotransmitter metabolism in vivo: on the correlation of total glucose consumption with glutamatergic action. J. Cereb. Blood. Flow. Metab. 2002; 22(11): 1343–1351.
21. Frahm J, Merboldt KD, Hanicke W. Localized proton spectroscopy using stimulated echoes. J. Magn. Reson. 1987; 72(3): 502–508.
22. Passonneau JV, Lauderdale VR. A comparison of three methods of glycogen measurement in tissues. Anal. Biochem. 1974; 60(2): 405–412.
23. England JD, Regensteiner JG, Ringel SP, Carry MR, Hiatt WR. Muscle denervation in peripheral arterial disease. Neurology. 1992; 42(5): 994–999.
24. Naressi A, Couturier C, Devos JM, Janssen M, Mangeat C, de Beer R, Graveron-Demilly D. Java-based graphical user interface for the MRUI quantitation package. Magn. Reson. Mater. Physic. Biol. Med. 2001; 12(2–3): 141–152.
25. Vanhamme L, van den Boogaart A, Van Huffel S. Improved method for accurate and efficient quantification of MRS data with use of prior knowledge. J. Magn. Reson. 1997; 129(1): 35–43.
26. Choi IY, Tkac I, Ugurbil K, Gruetter R. Noninvasive measurements of [1-(13)C]glycogen concentrations and metabolism in rat brain in vivo. J. Neurochem. 1999; 73(3): 1300–1308.
27. Morgenthaler FD, Lanz BR, Petit J-M, Frenkel H, Magistretti PJ, Gruetter R. Alteration of brain glycogen turnover in the conscious rat after 5 h of prolonged wakefulness. Neurochem. Int. 2009; 55(1–3): 45–51.
28. Hendrich K, Garwood M, Merkle H, Ugurbil K. Spectroscopic imaging using variable angle excitation from adiabatic plane-rotation pulses. Magn. Reson. Med. 1991; 19(2): 496–501.